ELSEVIER

International Journal of Mass Spectrometry 178 (1998) 143–159

International Journal of Mass Spectrometry

Atomic force microscopy of structures produced by electrospraying polymer solutions

Victor N. Morozov*, Tamara Ya. Morozova[1], Neville R. Kallenbach

W.M. Keck Laboratory for Biomolecular Imaging, Department of Chemistry, New York University, New York, NY 10003, USA

Received 21 January 1998; accepted 29 May 1998

Abstract

Solutions of synthetic [poly(ethylene oxides), polyvinylpyrrolidone, polyacrylamide, and poly(vinylalcohol)] and natural linear polymers (single- and double-strand DNA) have been electrosprayed onto mica surface and imaged with an atomic force microscope. Depending on the electrospray ionization (ESI) conditions (concentration, solvent, sign of ion charge) each polymer studied could be imaged as globular or fibrillar forms. Globules were observed after electrospray (ES) of dilute solutions such as are routinely used in mass spectroscopy studies of polymers. An increase in the polymer concentration resulted in formation of larger multimolecular globular clusters, then extended fibers, presumably consisting of single (0.2–0.5 nm high) and multiple (>0.6 nm high) polymer strands. Further increase in the polymer concentration produced complex structures including branched fibers, "pins," and "beads-on-a-string." Formation of these structures is discussed in terms of known mechanisms of ESI. (Int J Mass Spectrom 178 (1998) 143–159) © 1998 Elsevier Science B.V.

Keywords: Electrospray ionization; Polymers; Single stranded DNA; Double stranded DNA; Atomic force microscopy (AFM)

1. Introduction

Electrospray ionization (ESI) has found broad application in mass spectrometry (MS) as a nondestructive method for producing gas phase ions of biological and synthetic macromolecules. ESI can preserve not only the primary structure of polymer molecules but also structures formed due to noncovalent interactions [1–4]. Electrospray ESI generated polymer ions have begun to find applications in technology and biotechnology for modification of surfaces [5] and surface coating [6]. However, the mechanisms of formation of polymer ions in ESI are still not fully understood [1,7]. Different ideas have been proposed to account for formation of ions in ESI [8–14], which we discuss below. Structures we observe range from globules at concentrations comparable to those used in MS to fibers and more complex species at higher concentrations. It is important to contrast our results with the larger scale fibrillar structures that result from electrostatic atomization of very concentrated polymer solutions (2–10%, w/w), conditions referred to as "electrospinning" [15–19]. These spun fibers can hardly be considered as poly-

* Corresponding author.

Permanent address: Institute of Theoretical and Experimental Biophysics of the Russian Academy of Sciences, Pushchino, Moscow Region, 142292 Russia.

PII S1387-3806(98)14083-6

mer ions, since they consist of a great number of polymer chains forming threads with diameters ranging from tens to thousands of nanometers [15–19]. With a decrease in polymer concentration electrospinning is not observed, and normal ES resumes producing fine droplets.

Atomic force microscopy (AFM) has been previously used to visualize structures of natural [21] and synthetic [22,23] polymers. The products of ESI of dilute polymer solutions visualized by electron microscopy [20] or AFM [20,5] have always been reported to be globular. AFM has been applied to the visualization of structures formed by electrospray and electrospinning of polymer solutions. Jaeger et al. [18] used AFM to study electrospun PEO nanofibers deposited on a glass surface. Buchko et al. [5] imaged globular and fibrillar structures of a synthetic polypeptide after ES deposition on a silicon surface. Monomolecular globules and globular clusters of polystyrene formed in ES have been imaged on mica and graphite surfaces by Festag et al. [20]. AFM has also been used to study the structure of gas phase polymer ions indirectly, namely, by imaging surface defects induced on graphite and mica as a result of impact by incident energetic ions of PEO and proteins [24,25].

We use AFM in this work to visualize structures of different synthetic and biological polymer ions after different conditions of ESI and deposition onto mica surfaces. The surface of mica is atomically flat and enables observation of finer details of polymer structures than glass surfaces. Stability of images on mica greatly exceeds that on graphite since the former has sites capable of forming hydrogen and ionic bonds with hydrophilic polymer groups. The presence of a water layer on mica surfaces in contact with ambient air greatly reduces polymer binding, increases polymer thermal mobility, and thus reduces the stability of AFM images [26]. To prevent such motions and to favor droplet evaporation ESI has to be performed in a dry atmosphere, where the surface conductivity of mica, exploited in [20] vanishes. We describe here two methods that allow ES deposition of samples on mica in a dry atmosphere.

2. Experimental

2.1. Materials

Poly(ethylene oxide) with average molecular weight, $M_n = 8{,}000$ (PEO-8K), was purchased from USB Corporation. Other poly(ethylene oxides) with average $M_n = 1.0 \times 10^5$ (PEO-100K), $M_n = 4.0 \times 10^5$ (PEO-400K), $M_n = 2.0 \times 10^6$ (PEO-2M) and $M_n = 8.0 \times 10^6$ (PEO-8M) as well as poly(vinyl alcohol) (PVA-150K, average $M_n = 150{,}000$) were from Aldrich. Polyvinylpyrrolidone (PVP-360K, average $M_n = 3.6 \times 10^5$) was from Pharmacia. Polyacrylamide (PAM-5M, average $M_n = 5 \times 10^6$) was from Polyscience, Inc. Routinely, a stock solution of 1–10% concentration was prepared from the dry polymer by slowly shaking the tube for 4–12 h. Polymers of higher molecular weights [$(2-8) \times 10^6$] were shaken for more than 24 h. Aliquots of the stock solution were then diluted by solvent to required concentration and shaken again for at least 12 h before the ES deposition.

Methanol and acetonitrile of HPLC grade were obtained from Fisher Scientific. Water was deionized and then distilled. In some experiments water and water–methanol mixtures were filtered through a 0.2 μ Millipore filter.

DNA of λ-phage was obtained from New England Biolabs. A stock solution of DNA (containing 0.5 mg/mL) was washed twice with a ten-fold excess of water using an Amicon-100 microconcentrator and then used to prepare solutions. Na-polythymidylate-(poly[dT], $M_r = 600$ bases for 90% of molecules) was purchased from Sigma. To prepare stock solutions the dry sample was dissolved in water to a final concentration of 0.5–1 mg/mL and dialyzed overnight against water at 4 °C.

2.2. ES deposition

Two experimental arrangements used for ES deposition of polymers onto a mica surface are shown schematically in Figs. 1(A) and (B). Polymer solutions are sprayed from a glass or polyethylene capillary fitted with a tungsten, stainless steel, or platinum

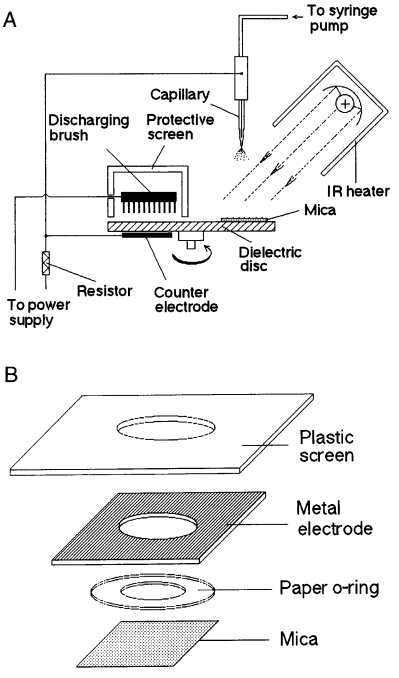

Fig. 1. Two methods used for ES deposition of polymer solutions. (A). Schematic of the device used for deposition onto dry mica surface in the "recharging" method. (B). Explosion view of arrangement for "sandwich" method of deposition using the surface conductivity of mica.

microelectrode. The design of the ES capillary was similar to that described in [27]. The outer diameter of the capillary was 30–50 μm. ES performance was visually monitored using a low power stereo-microscope. In most cases electrospraying was done in a "rainbow mode" that is characterized by production of uniform micron-sized droplets [12]. A microprocessor controlled syringe-pump (Cole-Parmer) in combination with a 10 mL Hamilton microsyringe were used to deliver polymer solution to the capillary with a constant flow rate that varied between 10 and 30 μL/h, in different experiments. The spacing between the capillary tip and mica surface was typically 35–40 mm.

As illustrated in Fig. 1(A) in the first ("recharging") method the mica sheet was placed onto a rotating plastic disc and periodically discharged when passing under an array of microelectrodes in a chamber shielded by a plastic screen. Positive or negative voltages could be applied to the capillary with respect to the mica. An IR heater or stream of dry warm air from a blow dryer was used to keep the mica dry during the ES deposition. Deposition could be performed either in open air or inside a plastic chamber with a controlled atmosphere. After deposition, mica was rapidly glued to a slightly heated metal disc and placed inside the AFM head, filled with dry air or nitrogen.

The second ("sandwich") method exploits the surface conductivity of mica. A mica sheet is brought into contact with a damp O-ring made of Whatman paper as illustrated in Fig. 1(B). The paper ring was covered with a metal electrode and a plastic screen both having a hole in the middle to enable free access of ions to the mica surface. ESI was performed in a closed plastic chamber through which a flow of dry air or oxygen was maintained. In some experiments ES deposition was made in an atmosphere free of carbon dioxide: air was bubbled through a saturated solution of $CaCl_2$, then dried by passing through tubes filled with solid NaOH and silica-gel. To adjust the humidity, part of the incoming gas stream was bubbled through a tube with CO_2-free water. Humidity and temperature inside the chamber were monitored with a digital humidity/temperature meter (Fisher Scientific).

2.3. Scanning

Images were recorded with a Nanoscope II (Digital Instruments, Santa Barbara, CA) instrument equipped with a 9 μm AFM head. Standard commercial Si_3N_4 cantilevers with highest compliance (nominally of 0.06 N/m) were used in most cases. Tips were made hydrophobic by treatment with dichlorodimethylsilane as previously described [28]. Imaging was performed under an atmosphere of dry air or nitrogen. A rubber o-ring placed on the scanner tube and a plastic plate on a front surface of the head formed a closed space inside the head which was kept dry by a flow of gas. Such a chamber enabled scanning of the same area of substrate before and after exposure of the sample to humid air, as well as scanning under different humidities. Temperature and humidity inside the head were controlled as described above for the ES chamber.

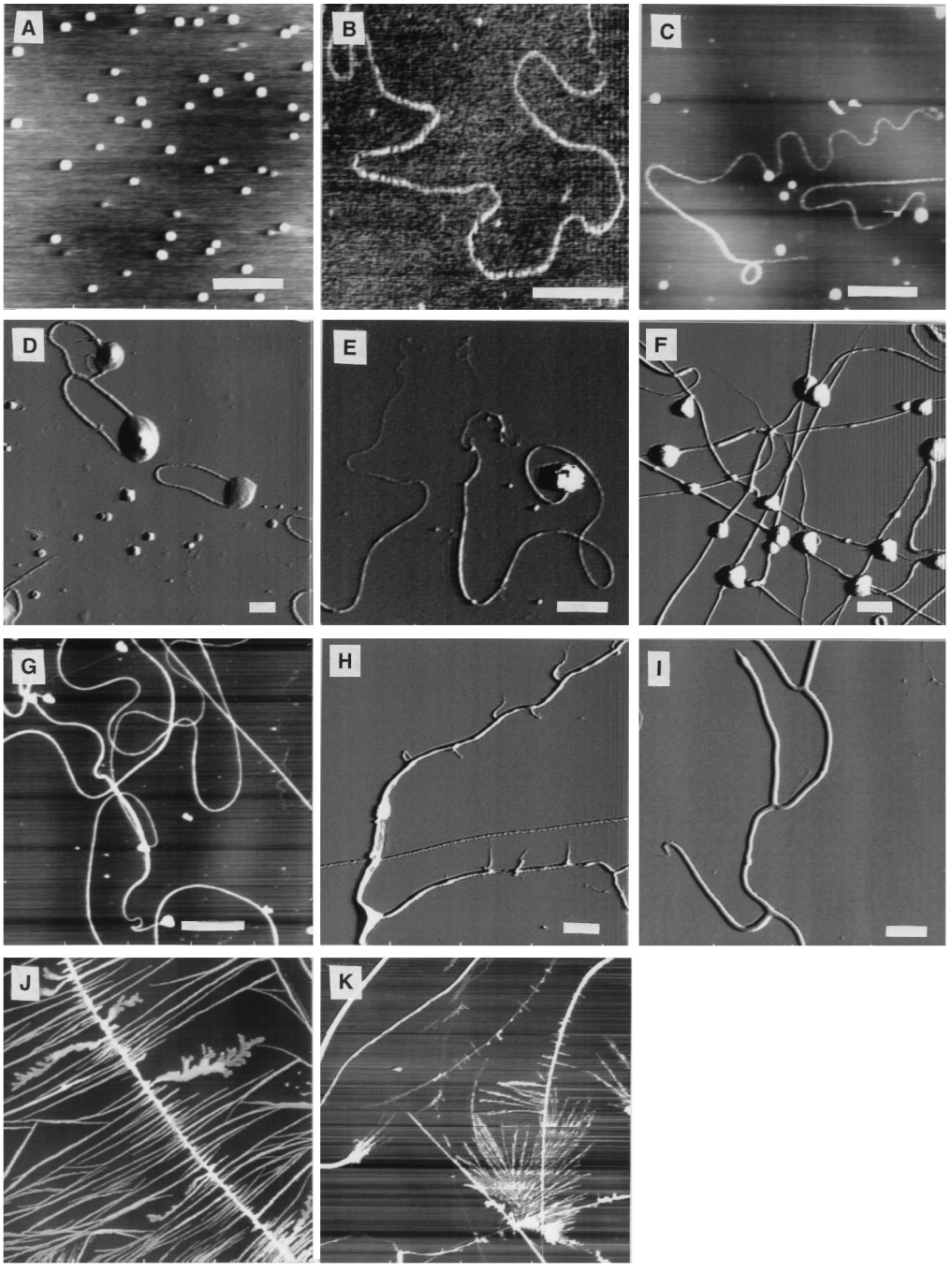

Fig. 2 (*caption on facing page*)

Before recording each image, scanning was performed under different forces (1–10 nN) on the cantilever to ensure that the measured height was not dependent upon the force. Routine scans were performed under the lowest force, i.e. 0.5–1 nN, which still allowed scanning in contact mode, without loss of tip/surface contact [26]. The scanning angle (the direction of scan with respect of the cantilever) was adjusted before each recording in the "Scope" mode until the forward and reverse traces were superimposed. This eliminates the artificial height contribution due to tip–surface friction [29,30].

The piezoscanner was calibrated in the *xy* plane using a square diffraction grid provided by the manufacturer. The scanner was calibrated in the *z* direction over a (0.340–2.05) μ range by the laser interference method [31]; this gave 9.03 $\pm$ 0.07 nm/V in good agreement with the 9.1 nm/V value specified by the manufacturer. Calibration on the nanometer scale was performed using gold beads (average diameter of 4.6 $\pm$ 0.6 nm) and polystyrene latex beads (average diameter of 35 $\pm$ 7.6 nm) both obtained from Sigma. A gold suspension containing 4.8×10^{13} particles/mL was diluted 200 times with water, applied on mica, and dried. Before application of a similarly diluted latex solution, the mica surface was coated with bovine serum albumin (BSA): 1 mg/mL solution of BSA was applied for 3 min on a freshly cleaved mica surface, blown off with nitrogen, washed with distilled water, and blown dry again. Measurements of 95 gold particles and 75 polystyrene beads gave average heights of 4.52 $\pm$ 0.76 nm and 34 $\pm$ 8 nm, respectively. Thus, all the calibrations were consistent within 3% with each other and with the values specified by the AFM manufacturer.

The images presented in this article show unprocessed data, except that in a few cases a flattening procedure was used.

3. Results

3.1. Morphology of structures and conditions for their formation

Some of the different types of structures resulting from ES of polymer solutions are presented in Fig. 2. The simplest structures are globules and fibers. Figs. 2(A) and (B) show globules of PEO-8M and a section of a PAM-5M fiber as examples.

Structures combining globular and fibrillar features are often observed together with simple globules and fibers as illustrated for DNA in Figs. 2(C) and (D) and for PVP in Fig. 2(E). They may consist of a fiber with a ball on one end or a loop protruding from a globule. We refer to both structures as "pins."

At high concentrations (1–10 mg/mL) some polymers (PEO, PVP and PVA) form structures consisting of large (up to 100–200 nm high) globules regularly positioned on a fiber, as shown in Fig. 2(F) for PEO-400K; we refer to these as "beads-on-a-string" or "necklaces." In some cases "whiskers" radiating from the capillary tip could be observed, both at-

Fig. 2. AFM images of synthetic and natural polymers electrosprayed on mica surfaces under different conditions. (A) PEO-8M globules ES deposited from 0.001 mg/mL solution in 50% MeOH, +4.3 kV at the capillary. Mica was heated with flow of warm air. (B) Part of a single-strand fiber of PAM-5M deposited from 0.01 mg/mL solution in water with the "recharging" method, +5.0 kV at the capillary (C) λ-DNA fibers ES deposited from 0.05 mg/mL solution in 90% acetonitrile at −9.8 kV on the capillary. (D) "Pins" of λ-DNA found in the sample prepared as described in (C). (E) "Pins" of PVP-360K obtained at −6.0 kV from solution of 0.1 mg/mL in 99% ethanol. (F) "Beads-on-string" structures prepared by ES of PEO-400K solution of 10 mg/mL in water. Potential at the capillary was +5.5 kV. (G) PAM-5M fibers electrospun from 0.1 mg/mL solution in water with +4.9 kV at the capillary. (H) Branched fibers of PAM-5M produced by ES of a 10 mg/mL solution in water at +7.0 kV. (I) Branched structures of PVA-150K obtained from a 10 mg/mL solution in water at +7.8 kV at the capillary. (J) Large "shish-kebob" and dendritic structures of PEO-8M found on mica after ES of 2 mg/mL solution in water at +6 kV. ES in air with relative humidity of 44%. (K) "Shish-kebobs," "whisks," and fibers found on mica after deposition of PEO-2M solution (1 mg/mL) in water. Voltage at the capillary is +3.8 kV. Air humidity is 7%. The "recharching" method was used to deposit the polymer structures in all cases except for (G) and (K) which used the "sandwich" method. The images in (D), (E), (F), (H), and (I) were taken in the "force" mode, the rest in the "height" mode. Bars corresponding to 0.5 μm in (A), (B), (E), and (D) and to 1.0 μm in all other pictures are included. Grayscales for images in the "height" mode are: 4 nm for (A), (C), (G), and (K); 1 nm for (B); and 12 nm for (J) The grayscale for images in "force" mode is: 0.001 nN for (H) and (I); 0.07 nN for (F); and 0.15 nN for (E) and (D).

Table 1
Conditions for formation of different structures in ES of polymer solutions

Polymer	Solvent	Concentration [a] nM	Voltage kV	Structures observed [b]
PVP-360K	EtOH 100%	**28**	+4.5	G, F
	Same	280	+4.0	F
	Same	2.8×10^3	+4.0	F, W
	Same	28	−4.8	G
	Same	**280**	−6.0	G, P, N
	MeOH 50%	0.28	+3.0	G
	Same	**2.8**	+4.0	G, F, P
	Same	28	+3.2	F, P
	Same	280	+8.0	F, P, W
	Same	2.8×10^4	+5.9	F, N
PAM-5M	Water	0.2	+7.0	G
	Same	**2.0**	+5.0	G, F
	Same	20	+4.9	F
	Same	200	+6.0	F
	Same	2.0×10^4	+7.0	F, B, W
PVA-150K	Water	67	+6.6	G
	Same	**670**	+6.6	G, F
	Same	6.7×10^3	+6.6	F, P, N
	Same	6.7×10^4	+7.8	F, B, W
λ-DNA [c]	Water	0.32	+4.5	G
	Same	3.2	+8.0	G
	AN 90%	0.32	−6.5	G
	Same	**3.2**	−9.8	F, P, W
	Same	3.2	−8.0	G, F, W
	AN 85%	3.2	−8.0	G
Poly[dT] [d]	AN 46%	270	−9.0	F, P
	Same	270	+7.0	G

[a] Concentrations, C_F, at which transition from fibrillar to globular ESI products occur are denoted with bold font.
[b] Meaning of the abbreviations used: G—globules, F—fibers, B—"brushes," P—"pins," N—"beads-on-string" or "necklaces," and W—"whiskers," seen at the capillary upon ES. EtOH, MeOH, and AN are ethanol, methanol, and acetonitril, respectively.
[c] Concentration attributed to one λ-DNA strand ($15{,}75 \times 10^6$ D) is presented.
[d] Average molecular weight of 193 kDa is taken to calculate concentration.

tached to the capillary walls and ejected from the Taylor cone as first described by Baumgarten [15].

Except for PVP, all the polymers studied here were found capable of forming branched structures upon ES of concentrated polymer solutions (10 mg/mL). These structures are illustrated in Figs. 2(H)–(K).

No difference was noted in the polymer structures when ES deposition was performed on mica in the "recharging" [Fig. 1(A)] or "sandwich" [Fig. 1(B)] method, unless the humidity of gas was allowed to exceed 25%, nor did we detect any differences in structure when ES was performed in a dry atmosphere free of CO_2 or in pure oxygen. We found it crucial to maintain low humidity (routinely about 6–20%) during all steps: deposition, transfer of the sample to the AFM head, and scanning itself, because exposure to atmosphere with humidity higher than 50% caused drastic changes in samples.

Table 1 presents some results specifying conditions under which different structures were observed with the polymers studied. A general phenomenon is clearly seen: any polymer studied can be imaged both in globular and in fibrillar form with any of the solvents used. A second general observation is the disappearance of fibrillar structures and appearance of globular ones when the concentration of polymer solutions falls below a certain level. As Table 1 and Fig. 3 show, the concentration, C_F, at which fibers begin to appear varies over a very broad range, from 2 nM for PAM-5M in 50% MeOH to 125 μM for

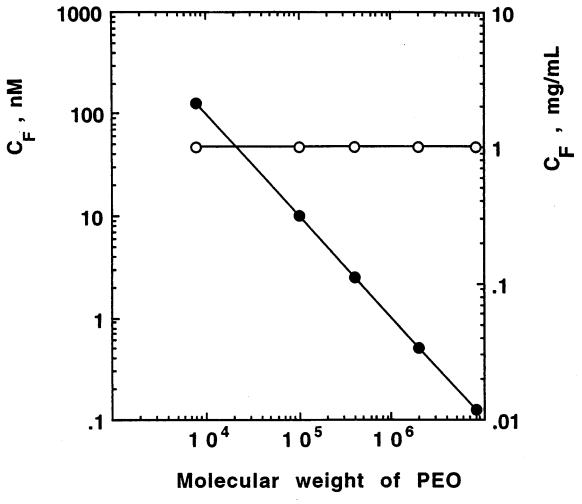

Fig. 3. The PEO concentration at which formation of fibers in ES begins, C_F, as a function of molecular weight of PEO. Filled circles correspond to C_F expressed in nM. Open circles show C_F in mg/mL. All solutions are prepared in water.

PEO-8K in water. This difference in C_F for different polymers diminishes 60-fold if polymer concentrations are expressed in mg/mL and completely disappears for water solutions of different PEOs, as seen from Fig. 3. The latter fact suggests that the total amount of polymer material per volume unit is important for fiber formation in ESI, rather than the *number* of molecules. This point is discussed further below, in considering different mechanisms of ion formation from linear polymers.

Table 1 shows that C_F depends on properties of polymer molecules, solvent, and the sign and value of potential at which deposition is performed. Thus, PVA and PAM sprayed from water solutions form fibers at concentrations of 0.1 mg/mL for PVA and 10^{-3} mg/mL for PAM, respectively one and three orders of magnitude lower than that for PEOs sprayed under the same conditions.

The role of solvent can be demonstrated with ES of PEO solutions. Exchange of water for 50% MeOH as solvent for PEO resulted in about a tenfold decrease in C_F. In contrast to water solutions, C_F in 50% MeOH becomes slightly dependent on the molecular weight of PEO. Thus, PEO-8T does not form fibers at the highest concentration tested, 0.5 mg/mL; PEO-100K produces only "pins" at such concentration, whereas PEO-400K, PEO-2M, and PEO-8M form fibers at 0.1 mg/mL. Another example of drastic changes in the ES product with solvent and concentration is observed in ES of DNA solutions: only globules are found after ES of 0.05 mg/mL solution of λ-DNA in 85% acetonitrile (AN), whereas a solution of the same concentration in 90% AN produced numerous "pins" and extended fibers [see Figs. 2(C) and (D)]. ES of the λ-DNA solution in 90% AN after ten-fold dilution produced no fibers at all. No fibers could be detected when λ-DNA was sprayed from water solutions.

The effect of sign of the ionic charge on C_F is illustrated by the behavior of poly[dT] and PVP. As seen from Table 1, ES of poly[dT] from a solution of 0.05 mg/mL in 46% AN results in formation of fibers at negative potential at the capillary, while only globules are formed at positive potential. The same is true for λ-DNA solutions. In contrast to poly[dT] and λ-DNA, PVP tends to unfold more readily at positive potentials. The effect of the potential is seen by ES of 0.05 mg/mL solution of λ-DNA in 90% AN, which shows complete disappearance of globular ES products upon increasing the potential from −8 kV to −9.8 kV.

Though the viscosity of polymer solutions has been implicated as a major factor controlling the process of electrospinning [15,17], our results indicate that viscosity does not determine the concentration at which fiber formation occurs in ES. For example, water solutions of PEO-8K and PEO-8M have similar values of $C_F = 1$ mg/mL despite a 3.5-fold difference in viscosity. On the other hand, a 10^{-3} mg/mL solution of PVP-360K in 50% MeOH formed fibers, whereas a solution twice as viscous, 0.5 mg/mL PEO-100K in the same solvent, did not. We will next consider various structures of the ES deposited polymers in more detail.

3.2. Fibers

Fibers have not been reported in ES of highly diluted polymer solutions or in control experiments with ES of solvents. The diameter of fibers measured by their height in AFM images increases considerably

with increase in polymer concentration. Much thinner fibers (0.3–10 nm) are observed here in ES of 0.001–0.1 mg/mL solutions than those formed from concentrated solutions (10–40 mg/mL) used in elecrospinning (40–2000 nm in diameter) [15–19]. The thinnest fibers found for all the polymers studied have a height in the range of 0.2–0.4 nm that presumably corresponds to single-strand polymer chains. An example of such a strand is shown in Fig. 2(B). It should be stressed, however, that such thin fibers are never found alone: they always were observed together with or as part of thick multistrand fibers.

An increase in humidity to $A = 30\%$ produced no visible changes in the fiber images. When exposed to $A = 58\%$ for 20 s and then dried again under nitrogen, PEO fibers thicker than 3 nm were unchanged. However, the thinner fibers disappeared, either forming flat disks or arrays of smaller flat particles tracing the position of the mother fiber. This suggests that polymer chains become mobile under exposure to humid atmosphere and can adopt relaxed forms.

3.3. DNA

As in the previous cases, ESI of DNA solutions produces globular and fibrillar structures depending on the ES conditions. Similar structures were observed for both single- and double-stranded DNA molecules. Spraying under a positive potential from water solutions always resulted in formation of globules only. Thus, ES of λ-DNA from a 0.05 mg/mL solution in water at positive voltage (conditions similar to those used in mass spectrometry studies, [32,33]) produced compact globules 20 ± 8 nm high. By contrast, ES from solutions in AN under negative potential produced fibers and "pins" similar to those seen in synthetic polymers [Figs. 2(C) and (D)]. As with the synthetic polymers, the average height of DNA varies along a fibril: the thinnest fractions have heights of 0.24 ± 0.05 nm and may represent single strands [34], in contrast to regions with greater thickness (from 0.5 ± 0.1 nm to 5 nm), which seem to be double and multistranded, respectively [34,35]. Occasionally, whole fibers of poly(dT) can be observed with the thickness and length expected for an extended single-strand molecule.

3.4. Complex fiber structures

Apart from unbranched fibers, more complex structures are observed when polymer solutions of 1–10 mg/mL concentration are sprayed. "Pins" appear to reflect some intermediate stage in formation of fibers. This form has been observed for PVP, PVA, PEO, and DNA. "Necklaces" or "beads-on-strings" similar to those shown in Fig. 2(F) for PEO-400K are observed for other PEOs and for PVA and PVP sprayed from concentrated water solutions with a positive potential at the ES capillary (see Table 1). This form has been recently described for PEO by Jaeger et al., [18] who suggested a possible mechanism for its formation involving transformation of an unstable water layer around the fiber into a series of water microdroplets.

Branched forms of fibers such as those illustrated in Figs. 2(H) and (I) are typical for PAM and PVP, but have been never found for the other polymers studied. These branched forms seem to occur in the gas phase, since branches often intersect the main fiber, and appear to be bent or broken, which would be expected to happen upon colliding with mica surface. Branches are separated by nearly equal intervals and may originate from some form of instability in charged fibers (see theoretical calculations in [36]).

PEO was the only polymer which formed the brushlike structures seen in Figs. 2(J) and (K). In contrast to the branches described above for PVP and PAM, those in PEO protrude nearly perpendicularly to the main chain and are often seen with thin dendritic structures [see Fig. 2(J)]. If these features arise in the gas phase, they should be altered or damaged upon hitting the surface. In fact, the branches neither look damaged nor cross each other or the main fiber. This is why we suppose that PEO branches are formed after the wet charged fiber collides with the mica surface. This hypothesis is supported by observation of much longer "brushes" when ES was performed at 44% humidity [Fig. 2(J)] as compared with spraying at 7% [Fig. 2(K)]. We also

found that short exposure of the ES deposited PEO sample to air with humidity of about 70% caused growth of additional perpendicular branches from the globules on fibers. Further increases in humidity resulted in transformation of all beads into lamellar brushes. We conclude therefore that PEO "brushes" are a crystalline form of this polymer known in morphology of fibrous polymer crystals as "shish-kebob" [37]. "Shish-kebob" structures of PEO were also described [38].

3.5. Globular structures

In contrast to fibrillar structures, globular particles are always observed upon ES of diluted polymer solutions. A small number of globules with dimensions comparable to those found in ES deposition of polymer solutions can also be observed in experiments with pure solvents, especially if water is used as solvent and deposition is performed in ambient air with a glass capillary enclosing stainless steel or tungsten electrodes. Some of these particles seem to serve as seeds for carbonate crystals that turn into well formed microcrystals after 5–10 days of mica storage in air over silica gel. To diminish the contribution of such artifactual particles, ES deposition was performed either in pure oxygen or in air passed through a CO_2-adsorber. It was also noted that use of a plastic (polyethylene) capillary and a platinum electrode greatly reduced both the size and number of particles in control experiments. Histograms of height distributions of particles found after ES of solutions of different PEOs in 50% MeOH are presented in Fig. 4 together with a control histogram of the solvent. It can be seen that the presence of a relatively small fraction of artifactual particles does not interfere with observation of polymeric globules. The rather broad distribution of heights among the polymer globules may reflect (1) polydispersity of the polymer sample, (2) different level of flattening, and (3) presence of intermolecular clusters. Despite all these factors, the measured average height of polymer globules tends to increase roughly in proportion to the 1/3 power of the mean molecular weight of polymer, as Fig. 5 indicates. This dependence confirms that globules elec-

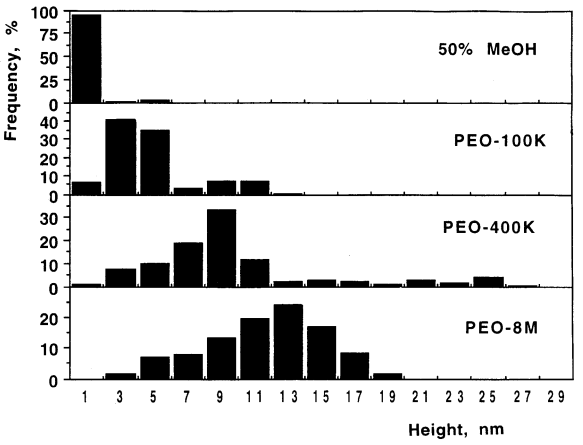

Fig. 4. Histograms of heights of PEO globules measured with AFM. Each histogram corresponds to measurements of 100–300 different particles. PEO-8M and PEO-400K were ES deposited from 1 nM solution and PEO-100K from 10 nM solution in 50% MeOH. The "sandwich" method of deposition was used to obtain these data. Deposition was performed at a relative humidity of 7–19%.

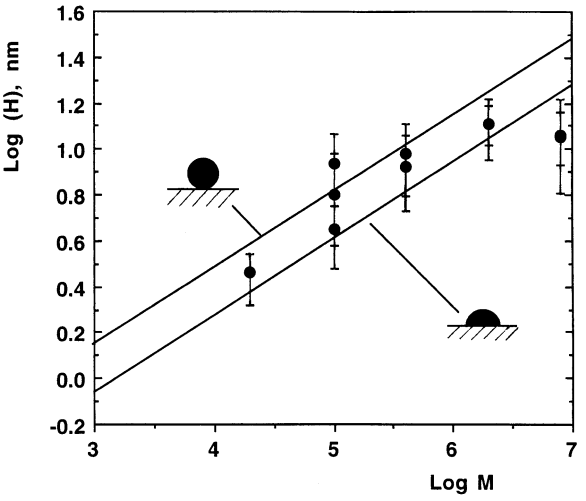

Fig. 5. Dependence of the average height of globules on the molecular mass of PEO. PEO globules were imaged after ES of 1–25 nM PEO solutions in 50% MeOH. Both "recharging" and "sandwich" methods were used. ES was carried out in air with a humidity between 6 and 30% in different experiments. Heights of 100–300 globules were measured in each experiment. The upper and lower lines correspond to theoretical estimates of height assuming spherical and hemispherical shapes of the globules, respectively. (The density of amorphous PEO was taken as 1.126 g/cm^3 [40]).

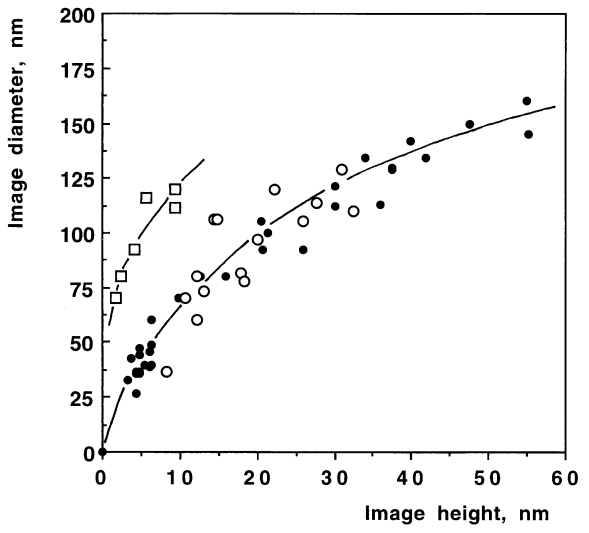

Fig. 6. Dependence of measured image diameter on image height for a series of spherical gold and polystyrene particles (filled circles), and for comparison, PEO-8M globles after ES deposited on mica (empty circles). Squares correspond to PEO globules in the same sample after exposing it to air with humidity of 58% for 20 s. All measurements were performed with the same tip.

trosprayed from diluted (1–25 nM) solutions consist mostly of single polymer molecules and that no considerable damage to these molecules occurs during the ESI and deposition. Two theoretical lines in Fig. 5 are calculated for each molecular weight assuming that the PEO globules are spheres (upper line) or hemispheres (lower line) with a density of the amorphous bulk polymer [39], ρ = 1,126 g/cm^3. The majority of the experimental points in Fig. 5 fall between the two theoretical lines, indicating that globules are not precisely spherical. This deviation from sphericity increases with the size of PEO globules. A similar flattening in the case of larger polystyrene globules was noticed by Festag et al. [20]. Data presented in Fig. 6 also support the idea that polymer globules can be described as spherical or hemispherical particles, since they are characterized by the same ratio of effective AFM diameter to AFM height as gold and polystyrene spherical beads imaged with the same tip. It is difficult to distinguish between spheres and hemispheres based only on measurements of height and effective lateral diameter: when the tip radius exceeds the radius of particles, they tend to show nearly the same profile.

Globules formed in ES do not show any changes in height or form upon sample storage in dry argon and scanning if the relative humidity is kept below A = 40%. A distinct decrease in globule height (2–3-fold) occurs after a brief, 20 s, sample exposure to a humidity of A = 58%. As seen in Fig. 6, the particles flatten considerably judging from their quite different ratios of height to diameter. This flattening of particles of hydrophilic polymers in a humid atmosphere may account for part of the measured spread in the heights of globules in Figs. 4 and 5. Exposure to still higher humidity resulted in transformation of globules into flat formless leaflets less than 1 nm high.

4. Discussion

4.1. Potential artifacts

One important issue to be addressed first is the possibility of artifacts in the imaging of our experiments. In contrast to the early studies by Sullivan et al. [25] and Reimann et al. [24] in which conclusions about the structure of ES generated polymer ions were based on analysis of surface defects originating from the impact of highly energetic polyions, the polyions in our experiments are deposited under much milder conditions—that is, normal pressure, without acceleration or exposure to high temperatures or high-energy collisions with gas molecules. The structures we observe on mica surfaces after ES deposition under mild conditions can be easily displaced by scanning with a large force. They also display a characteristic deformability which increases with increase in relative humidity up to 40–50%: the height of the structures begins to change at lower tip forces in humid conditions rather than in a dry atmosphere. These features lead us to conclude that the observed structures are not defects of the mica surface but real structures imaged on the intact mica surface.

AFM imaging of structures deposited under ES does not address the important question of whether the observed structures consist of polymer molecules.

The answer is clearly yes in cases where numerous similar fibrillar structures are observed in a field. However, the interpretation of globular structures at high dilution has to be more cautious. Solid residues of salts and other impurities present in solvents, products of dissolving the glass capillary, electrochemical reactions on the electrode, and carbonate microcrystals known to grow on mica surface in contact with ambient air [40,41], may all contribute statistically to observations of globular ES products. Based on control experiments with solvents, we have found that ES in an atmosphere free of carbon dioxide, and use of polyethylene capillaries with a Pt electrode rather than glass capillaries with a tungsten electrode, greatly reduce both the number and height of globules observed in controls. As seen in Fig. 5, the average height of PEO globules is proportional to the 1/3 power of the molecular weight of PEO, which shows that most of the globules consist of single polymer molecules.

It is worth noting that our conclusion that the polyions formed from diluted polymer solutions are globular is not affected by the possible presence of nonpolymeric globules among ES products, because fibrillar structures have never been found in control ES of solvents or in ES deposits from dilute polymer solutions. Still, the presence of nonpolymeric globules could pose a serious problem if one is interested in using ES deposition for microscopic analysis of polymer mass distributions, for example.

4.2. Site of formation of polymer structures

Do the structures we observe form in the gas phase or on the surface? In principle, both globular and fibrillar structures could be formed upon drying of a droplet of polymer solution on a surface. Karthaus et al. [42] have shown that a regular array of flat round particles with a height of 2–7 nm and diameter of ~300 nm is formed on a mica surface upon drying a layer of polystyrene solution in benzene. Richardson [43,44] has demonstrated formation of nearly spherical polymer globules on carbon-coated mica after evaporation of the solvent from microdroplets of diluted polymer solutions in poor solvents. However, only very flat disks and branched fibrillar structures radiating from them were seen if good solvents were used. Since only good solvents are used in our experiments we believe that the nearly spherical polymer particles observed here after ES deposition could only be formed in the gas phase prior to impact with the surface. Another argument supporting this conclusion is the relative instability of the structures observed in the presence of water used as a pure solvent or as a part of a solvent mixture in most of our experiments. As mentioned in the Results section above, even a brief (10–20 s) exposure of a sample to moderately humid air ($A = 58\%$) results in drastic flattening of globules and disappearance of thin fibers. Further increases in humidity cause complete disappearance of the above structures. Our estimates of the average diameter of a droplet and calculation of the evaporation time are presented in Appendix 1. The results suggest that water droplets of <1 μm in diameter, which are typically generated in our ES conditions, will completely evaporate during their 30–40 mm trajectory from capillary to substrate. Since thermal motion of polymer chains is greatly hindered in the absence of solvent [34,45], we believe that interconversion of globular and fibrillar polymer structures on the mica surface is unlikely, hence the observed structures could be formed in gas phase only. A further argument favoring our conclusion that formation of globular and fibrillar polyions occurs during ESI and not as a result of drying droplets on the surface is provided by the fact that globular structures (instead of fibrillar ones) always occur upon decreasing the polymer concentration below C_F, regardless of the properties of surface or solvent used. Thus, in addition to our experiments with polymer solutions in water, methanol, ethanol, and acetonitrile sprayed onto hydrophilic mica surfaces, polymeric globules have been detected on hydrophobic graphite surfaces [20], on crystalline gold [27], and on silicon [5], after ES deposition from dilute solutions in water, chloroform, and formic acid—solvents which differ tenfold in their saturation vapor pressure, threefold in surface tension, and 15-fold in their dielectric constant.

The smooth slightly wavy fibers seen in Figs. 2(B),

(C), (E), and (G) are never observed after drying polymer solutions on surfaces. This provides a further argument to confirm that fibers form in the gas phase. Additional arguments to indicate that thin polymer fibers (0.2–8 nm high) are not only formed in gas phase but have time to evaporate solvent before falling onto the mica surface are the following: (1) The characteristic bulges in zones of fiber crossing that are seen in the case of fibers that have been applied wet and then dried on surfaces [19] are absent; (2) the height of crossing of fibers agrees with the sum of the diameters of the crossing fibers; and (3) the lateral diameter of fiber images matches the diameters of standard polystyrene beads.

Thick fibers (10–60 nm high, such as those presented in Figs. 2(F), (H), and (I) are formed from polymer solutions at concentrations that are 4–10 times below those used in electrospinning [5,19,22]. Though undoubtedly formed in the gas phase also, these thick fibers seemingly do not completely lose solvent before deposition on the surface. The presence of flat ribbon fragments along the fiber in Fig. 2(H), the growth of dendritic crystals [see Figs. 2(K) and (J)] as well as the presence of "shish-kebob" type structures [37] are all consistent with the presence of solvent in or around the fibers.

The thrust of these arguments is that both the globular and fibrillar polymer structures we observe are formed in the gas phase rather than on the surface, and are unlikely to transform into each other if the mica surface is kept dry. This conclusion allows us to compare our data with the results from MS studies and to make certain inferences about some of the possible mechanisms of ESI.

4.3. Relation to MS studies

According to MS data, the average mass per unit charge in PEO ions is roughly the same (m/z = 600–1200) for polymer ions of different total molecular weight. This has been interpreted in terms of a model in which charges are distributed along the extended polymer chain [11–13]. Our experiments with ES of PEO solutions under conditions as close as possible to those used in mass spectroscopy studies (same concentration, solvent, sign and potential value, rate of solution flow) have never revealed a single fibrillar structure. The only reasonable explanation for this discrepancy is that fibrillar structures are formed in the mass spectroscopy experiments not by ESI itself, but upon subsequent dehydration of PEO ions and collision with gas molecules that are considerably stronger in the mass spectroscopy device than in our experiments. Polyions formed after ES fly in a counter-flow of dry nitrogen heated to 333 K in mass spectroscopy devices, and are subjected to collisions with gas atoms as they enter the vacuum chamber [46]. It is well known that three water molecules are bound per $-CH_2-CH_2-O-$ repeat unit in the PEO helix [47]. Stripping these water molecules might considerably destabilize PEO globules and facilitate their unfolding. Studies of protein ions using ion mobility mass spectrometry techniques show that even completely dehydrated protein ions can be unfolded when heated by high energy collisions in a vacuum [48–50].

4.4. Implications for ES mechanisms

The results presented above raise two important questions: (1) why is there always a critical concentration, C_F, below which fibrillar structures cannot be observed in our experiments or other reports [5,20]? and (2) why does the total concentration of monomer rather than other factors determine the condition for fiber formation? Available theories of ESI do not seem to answer these questions adequately.

At the present time, two different mechanisms of ion formation in ESI are discussed (see the excellent reviews by Kebarle and Tang [1] and Kebarle and Ho [7]). According to Dole, polyions are simply the residues left after evaporation of solvent from charged droplets [8,10]. This idea readily explains formation of globules. Fenn et al. [13] suggested, however, that extended polymer states must arise in ESI-MS in order to explain the constancy of mass-to-charge ratios for PEO samples of different mass. The alternative mechanism, proposed by Iribarne and Thomson, explains formation of ions as the result of field evaporation [9]. In this model, an ion can cross a

liquid/gas interface when the electric field on the droplet surface exceeds a critical level that is estimated to happen only for droplets of ~20 nm in diameter. Fenn's modification of this mechanism [13] explains formation of extended fibers in terms of a free end or loop which crosses the surface barrier due to thermal motion and is then further pulled by electrostatic forces. If this process is stopped for any reason "pins" should result. However, the images of "pins" presented in Figs. 2(C), (D), and (E) cannot be considered as a proof of this mechanism since the size of the globules at the fiber ends considerably exceeds the size of the droplets necessary for field evaporation. Moreover, this mechanism does not explain why fibers do not form when diluted solutions are sprayed. What inhibits formation of a fiber when only a single polymer molecule occupies a droplet? Estimates of the dimensions of random coiled polymer chains according to Flory [51] give values between 3 and 90 nm for the PEO samples of this study, close to or greater than the radius of droplets capable of field evaporation (8–13 nm, [9]). Increased viscosity or even solidification of the material in a droplet before the critical size is reached could make this mechanism unacceptable in describing formation of large polymer ions. Although the mechanism of field evaporation can account for formation of small organic or inorganic ions or ions in globular proteins with a size less than 10 nm, it seems unlikely to work in the case of high molecular weight linear polymers.

Formation of fibrillar structures might be explained by a different mechanism in which the end of a polymer or a loop penetrates through the surface of a charged droplet along with the flow of offspring microdroplets. Electrostatic repulsion could then drag the entire chain out of the droplet. This mechanism could operate in much larger droplets than those required for field evaporation. However, the absence of any traces of fibrillar structures among the ES products of diluted polymer solutions presents a difficulty for this mechanism too. We suggest instead that fibers might be formed in ES upon transition from the Taylor cone to a jet, the condition for their formation being the presence of tangled chains with an effective size exceeding the diameter of the jet. In our experiments we estimate that the diameter of the jet is about 500 nm (the diameter of the jet is 1.9-fold smaller than that of initial droplets [52], see Appendix 1). The latter value is significantly larger than the average diameter of a random coil of even the largest polymers used here (180 nm for PEO-8M). This could explain why fibers are not formed from dilute polymer solutions. The fact that C_F depends on the total concentration of monomers rather than the molecular weight of PEO provides a supportive argument for the necessity of chain entanglement and aggregation in formation of fibers in ESI.

5. Summary

In conclusion, we find that ES is capable of producing a much greater diversity of polymer structures than have been reported before. The range includes fibers with a thickness corresponding to the height of single polymer chains and regularly branched fibers. Some of these structures might find applications in polymer physics [20] and polymer technologies [53]. For example, the internal structure of membrane filters fabricated by ES deposition of polymer ions can be controlled by changing the concentration, solvent, or other parameters that determine whether fibrillar or globular structures will be deposited and thereby allow precise control of the size of polymer clusters. Formation of extended single- and double-stranded DNA fibers offers another example of current interest: ES deposition can be used to prepare extended DNA molecules for analysis of their sequence, binding by proteins, or mapping with STM, AFM, and other scanning probes capable of atomic resolution.

Acknowledgements

This work was supported by NSF grant no. BIR 9513571 and by NIH grant no. CA 24101.

Table 2
Size and charge of water/glycerol droplets generated upon ES

Glycerol w/w, %	Humidity	Height,[a] d, mm	V, kV	I, nA	$v_n^b \times 10^{-9}$	Radius μm	Q/Q_r^c
5	20	11	2.9	12	1.9 ± 0.6	0.50	0.40
5	20	20	3.1	12	1.3 ± 0.4	0.57	0.48
5	20	30	3.6	17	1.8 ± 0.6	0.51	0.29
5	20	38	4.3	17	2.4 ± 0.8	0.48	0.34
10	30	20	3.3	13	2.5 ± 0.8	0.46	0.29
10	88	20	4.3	10	2.7 ± 0.9	0.44	0.43

[a] Height denotes distance from capillary tip to substrate.
[b] $v_n = N/V_f \tau$, represents the number of droplets formed upon ES of 1 μL of solution.
[c] Rayleigh charge for given radius was calculated as $Q_r = 8\pi(\varepsilon_0 \gamma R^3)^{1/2}$, with ε_0 being the dielectric constant for vacuum and γ being surface tension of liquid. The latter value for 10% glycerol, $\gamma = 0.0729$ N/m at 18 °C is very close to that of water, $\gamma = 0.0730$ N/m.

Appendix
Estimation of evaporation time in ES deposition

1. Experimental estimation of average size of parent droplets

The size of a liquid droplet can be monitored optically only if it is large enough [54]. We have developed a simple method to allow estimation of average diameter of submicron droplets. The method relies on direct counting of droplets of nonvolatile liquid residues of electrosprayed droplets deposited onto an optically flat mirror surface. It is based on the assumption that only residues from parent micron sized droplets will be optically detectable, whereas those formed by drying of offspring droplets that have a volume of roughly 1/1000 of the parent's [54] will not be visible.

Glycerol solutions in water (5 and 10%, w/w) were electrosprayed under conditions typically used for ES deposition of polymers: a capillary with external tip diameter of 30 μm, flow rate of 0.2–0.3 μL/min, and voltage of 3–4 kV. Deposition was performed under low and high humidity at different distances, d, between the capillary tip and the substrate. ES was performed through a dielectric mask with a round hole 15 mm in diameter for a period sufficient to establish stable ES. The substrate was then shifted rapidly to expose a clean area for 2 s and then returned to its initial position. Neither the visual appearance of the ES torch nor the current revealed any changes upon such short-term substrate displacements.

The surface density of microdroplets collected during a 2 s period was measured with an optical microscope ($\times$30 objective) equipped with an epicondenser. Though droplets were beyond the optical resolution to measure their diameters directly, they can be easily counted to estimate the radial distribution of the surface density of droplets as well as the total number of droplets, N, in the deposit. Routinely, the number of droplets, $n_i(r)$ in five square fields of area $s = 9 \times 9 = 81$ μm^2 each, were counted and averaged. The substrate was then shifted by 1–2 mm along the spot diameter and the same counting procedure repeated. The radial distribution of droplet density that was obtained in this way was used to calculate the total number of droplets in the deposit by integrating over the area of the whole spot $N = s^{-1} n(r)\ 2\pi r dr$.

Data summarized in Table 2 show that variations in the number of droplets per volume unit of liquid ($N/V_f \tau$) do not exceed the experimental error despite considerable variation in the capillary-to-substrate distance, humidity, and glycerol content. Since the rate of droplet drying and the number of offspring droplets formed should change drastically with these changes in conditions, one may conclude that offspring droplets do not interfere with our measurement and that the procedure gives a reliable estimate of the

number of initial droplets and allows calculation of their mean radius:

$$R = [(3/4)\ V_f\ \tau/N]^{1/3} \quad (1)$$

Here V_f is volume flow rate of solution. As seen in Table 1, the average radius of mother droplets under our experimental conditions is $R = 0.49 \pm 0.05$ μm and does not show any significant dependence on the humidity, height, or glycerol concentration.

From the known current, I, the initial average charge on the mother droplets, Q, can also be calculated:

$$Q = I\tau/N \quad (2)$$

Two independent arguments support the reliability of the above estimate of droplet size and explain the lack of effect of glycerol. Extrapolation of the curve presented in Fig. 6 of [55], describing the experimentally measured diameters of water droplets as a function of flow rate, V_f, for corona-assisted ES, gives a diameter of less than 1 μm for the value of V_f we used. The relation of the average charge on the initial droplet to its Rayleigh limit, $Q/Q_r = 0.37 \pm 0.08$, is also in good agreement with data published in the literature for ES of deionized water: $Q/Q_r = 0.35$ according to [56].

We used different formulas available in the literature to theoretically predict the expected diameter of parent water droplets. Of the known equations used (Pfeifer and Hendricks [57], Fernandez de la Mora and Locetales [58], Gannan-Calvo [59]) only the expression derived by Wilm and Mann [60] seems consistent with our measurements. According to this latter work the radius of a jet is:

$$R_j = \{\rho/[4\pi\gamma \tan(\pi/2 - \theta)[(U_a/U_t)^2 - 1]\}^{1/3} V_f^{2/3} \quad (3)$$

Substituting values of the density, $\rho = 1000$ kg/ms, surface tension of water, $\gamma = 0.07$ N/m, ratio of voltage actually operated in our ES to the threshold voltage, $U_a/U_t = 1.1$, and cone half-angle, $\theta = 49°$, we obtain for the radius of jet: $R_j = 0.37$ μm, which is close to our experimental estimate for the radius of the droplets.

2. Estimation of evaporation rate and path for charged water droplet

The theory of droplet evaporation has been well developed [61,62]. Evaporation of small droplets, with $R \ll \lambda/\chi$, is not predicted to be influenced by droplet motion. If the mean free path of gas molecules is $\lambda = 0.07$ μm and the condensation coefficient for water, $\chi = 0.04$, this condition is satisfied for water droplets with $R \ll 1.7$ μm in air under normal conditions. Evaporation of such a droplet then follows the equation [63]:

$$R(t) = R_o - \alpha t \quad (4)$$

where

$$\alpha = (v_s \chi \mu n_s/4\rho)\ (1 - A) \quad (5)$$

Here v_s is the average thermal velocity of water molecules in the gas phase, n_s is the concentration of the saturated vapor at the droplet temperature (for a water droplet with $R \leq 0.5$ μm the difference between this temperature and the temperature of gas phase does not exceed 5 K [62]), μ is the mass of solvent molecule and $A = n/n_s$ is the relative humidity in the case of water. Taking into account that at a room temperature of 298 K a water droplet has an actual temperature of 293 K and with $v_s = 5.9 \times 10^2$ m/s, $\mu = 3 \times 10^{-26}$ kg, $n_s = 7.46 \times 10^{23}$ m^{-3} we obtain $\alpha = 96$ μm/s for $A = 0$ and $\alpha = 72$ μm/s at $A = 25\%$. This means that the total time required to evaporate a droplet with initial radius of 0.5 μm is $\tau_0 = 5.2$ ms at $A = 0$ and $\tau_0 = 6.9$ ms at $A = 25\%$.

To estimate the distance of flight of the evaporating and decaying charged droplet we assume that droplets move in a constant electric field, E, that is equal to the mean of the actual field present. The latter value can be calculated using a point-to-plane approximation of the actual field [64]:

$$E = V/d \quad (6)$$

where V and d are potential difference and distance between capillary and substrate, respectively.

The electrophoretic mobility, Z, of the charged

spherical droplet in a gas with viscosity, η, is a function of its radius [64]:

$$Z = (QE/6\pi\eta R)[1 + (\lambda/2R)] \times [2.51 + 0.80 \exp(-1.1R/\lambda)] \quad (7)$$

which at $\lambda \ll R$, reduces to the simple Stokes equation:

$$Z = (QE/6\pi\eta R) \quad (8)$$

To obtain this equation of motion for a droplet in an electric field we also neglect loss in mass as the droplet decays (since each of them takes only about 2% of droplet mass) and assume that as the radius of the droplet decreases its charge is reduced by the same fixed fraction, β, of the Rayleigh limit, Q_r, for each radius:

$$Q(R) = \beta Q_r = 8\pi\beta(\varepsilon_0\gamma R^3)^{1/2} \quad (9)$$

where γ is surface tension and ε_0 is the permittivity of vacuum. The validity of this assumption is supported by known experimental data, according to which a droplet decays when its charge reaches $0.7Q_r$ and in each decay it loses about 15% of its charge and 2% of its mass, thus reducing its charge to $0.61Q_r$. We thus take an intermediate value of $\beta = 0.65$ as an estimate.

From Eqs. (8), (9), (6), and (4) we obtain an equation for the motion of an evaporating droplet:

$$(dx/dt) = 4\beta V[\varepsilon_0\gamma(R_o - \alpha t)]^{1/2}/3\eta d \quad (10)$$

Solving this equation gives for the maximum travel of a droplet before it evaporates completely:

$$X_{\max} = 8\beta V(\varepsilon_0\gamma R_o^3)^{1/2}/9\eta d\alpha \quad (11)$$

With viscosity of air, $\eta = 1.84 \times 10^{-5}$ kg/ms, $\gamma = 0.07$ N/m, $V = 4.3$ kV, $d = 38$ mm, and all other parameters as above indicated, we find $X_{\max} = 9.5$ mm at $A = 0\%$ and $X_{\max} = 12.7$ mm for $A = 25\%$. Because this distance is about 3–4 times smaller than the distance between the capillary tip and the mica surface, $d = 30$–40 mm used in actual experiments, this estimate shows that submicron water droplets should evaporate well before they reach the substrate surface.

References

[1] P. Kebarle, L. Tang, Anal. Chem. 65 (1993) 973A.
[2] R.D. Smith, J.E. Bruce, Q. Wu, Q.P. Lei, Chem. Soc. Rev. 26 (1997) 191.
[3] C.V. Robinson, S.E. Radford, Structure 3 (1995) 861.
[4] M. Przybylski, M.O. Glocker, Angew. Chem. Int. Ed. Engl. 35 (1996) 806.
[5] C.J. Buchko, K.M. Kozloff, A. Sioshansi, K.S. O'Shea, D.C. Martin, in C.M. Cotell, A.E. Meyer, S.M. Gorbatkin, G.L. Grobe III (Eds.), Thin Films and Surfaces for Bioactivity and Medical Applications, MRS, Pittsburgh, PA, 1996, p. 23.
[6] B. Hoyer, G. Sørensen. N. Jensen, D.B. Nielsen, B. Larsen, Anal. Chem. 68 (1996) 3840.
[7] P. Kebarle, Y. Ho, in R.B. Cole (Ed.), Electrospray Ionization Mass Spectrometry, Wiley, New York, 1997, Chap. 1.
[8] M. Dole, L.L. Mack, R.L. Hines, R.C. Mobley, L.D. Ferguson, M.B Alice, J. Chem. Phys. 49 (1968) 2240.
[9] J.V. Iribarne, B.A. Thomson, J. Chem. Phys. 64 (1964) 2287.
[10] L.L. Mack, P. Kralik, A. Rheude, M. Dole, J. Chem. Phys. 52 (1970) 4977.
[11] S.F. Wong, C.K. Meng, J.B. Fenn, J. Phys. Chem. 92 (1988) 546.
[12] T. Nohmi, J.B. Fenn, J. Am. Chem. Soc. 114 (1992) 3241.
[13] J.B. Fenn, J. Am. Soc. Mass Spectrom. 4 (1993) 524.
[14] J.B. Fenn, J. Rosell, T. Nohmi, S. Shen, F.J. Banks Jr., in A.P. Snyder (Ed.) Biochemical and Biotechnological Applications of Electrospray Ionization Mass Spectrometry, ACS, Washington, DC, 1996, Chap. 3.
[15] P.K. Baumgarten, J. Colloid Interface Sci. 36 (1971) 71.
[16] L. Larrondo, R.S.J. Manley, J. Polym. Sci. 19 (1981) 909, 921, 933.
[17] J. Doshi, D.H. Reneker, J. Electrost. 35 (1995) 151.
[18] R. Jaeger, H. Schönherr, G.J. Vancso, Macromolecules 29 (1996) 7634.
[19] D.H. Reneker, I. Chun, Nanotechnology, 7 (1996) 216.
[20] R. Festag, S.D. Alexandratos, K.D. Cook, D.C. Joy, B. Annis, B. Wunderlich, Macromolecules 30 (1997) 6238.
[21] STM and SFM, in O. Marty, M. Amrein (Eds.), Biology, Academic, New York, 1993.
[22] S.N. Magonov, D.H. Reneker, Annu. Rev. Mater. Sci. 27 (1997) 175.
[23] See also the series of papers published in ACS Polymer Reports, 37 (1996) 550.
[24] C.T. Reimann, A.P. Quist, J. Kopnczky, B.U.R. Sunqvist, R. Erlandsson, P. Tengvall, Nucl. Instrum. Methods Phys. Res. B 88 (1994) 29.
[25] P.A. Sullivan, J. Axelsson, S. Altmann, A.P. Quist, B.U.R. Sunqvist, C.T. Reimann, J. Am. Soc. Mass Spectrom. 7 (1996) 329.
[26] C. Bustamante, J. Vesenka, C.L. Tang, W. Rees, M. Guthold, R. Keller, Biochemistry, 31 (1992) 22.
[27] V.N. Morozov, N.C. Seeman, N.R. Kallenbach, Scanning Microsc. 7 (1993) 757.
[28] J.S. Berger, J.A. Ernst, A.C. Nicoletta, L.A. Hull, J. Yang, R. Qiu, V.N. Morozov, N.R. Kallenbach, J. Biomol. Struct. Dyn. 14 (1996) 285.

[29] Y.L. Lyubchenko, P.I. Oden, D. Lampner, S.M. Lindsey, K.A. Dunher, Nucl. Acids Res. 21 (1993) 1117.
[30] W.L. Shaiu, D.D. Larson, J. Vesenka, E. Anderson, Nucl. Acids Res. 21 (1993) 99.
[31] M. Jaschke, H.J. Batt, Rev. Sci. Instrum. 66 (1995) 1258.
[32] R. Chen, X. Cheng, D.W. Mitchell, S.A. Hofstadler, Q. Wu, A.L. Rockwood, M.G. Sherman, R.D. Smith, Anal. Chem. 67 (1995) 1159.
[33] X. Cheng, D.G. Camp II, Q. Wu, R. Bakhtiar, D.L. Springer, B.J. Morris, J.E. Bruce, G.A. Anderson, C.G. Edmonds, R.D. Smith, Nucl. Acids Res 24 (1996) 2183.
[34] T. Thundat, D.P. Allison, R.J. Warmack, J. Vac. Sci Technol. A 11 (1993) 824.
[35] Y.L. Lyubchenko, L.S. Schlyakhtenko, Proc. Natl. Acad. Sci. USA 94 (1997) 496.
[36] A.A. Shutov, A.A. Zakhar'yan, Phys. Dokl. 42 (1997) 451.
[37] B. Wunderlich, Macromolecular Physics, Academic, New York, 1973, Vol. 1.
[38] Z. Pelzbauer, R.S.J. Manley, J. Macromol. Sci., Phys. B 4 (1970) 761.
[39] P. Malyneux, Water Soluble Polymers: Properties and Behavior, CRC, Boca Raton, FL, 1983, Vol. 1, p. 22.
[40] H.K. Christenson, J.N. Israelachvili, J. Colloid Interface Sci. 117 (1987) 576.
[41] J.N. Israelachvili, G.E. Adams, J. Chem. Soc., Faraday Trans. 74 (1978) 975.
[42] O. Karthaus, K. Ijiro, M. Shimomura, Chem. Lett. (1996) 821.
[43] M.J. Richardson, Nature, 198 (1963) 252.
[44] M.J. Richardson, J. Polym. Sci., Part C: Polym. Symp. 3 (1963) 21.
[45] B. Samori, C. Nigro, A. Gordano, I. Muzzalupo, C. Qagliariello, Angew. Chem. Int. Ed. Engl. 35 (1996) 529.
[46] C.B. Jasieczek, A. Buzy, D.M. Haddleton, K.R. Jennings, Rapid Commun. Mass Spectrom. 10 (1996) 509.
[47] K.-J. Liu, J.L. Parsons, Macromolecules 2 (1969) 529.
[48] S.J. Valentine, J.G. Anderson, A.D. Ellington, D.E. Clemmer, J. Phys. Chem. B 101 (1997) 3891.
[49] K.B. Shelimov, M.F. Jarrold, J. Am. Chem. Soc. 118 (1996) 10 313.
[50] K.B. Shelimov, D.E. Clemmer, R.R. Hudgins, M.F. Jarrold, J. Am. Chem. Soc. 119 (1997) 2240.
[51] P.J. Flory, Statistical Mechanics of Chain Molecules, Wiley, New York, 1969.
[52] K. Tang, A. Gomez, Phys. Fluids 6 (1994) 2317.
[53] See references for possible applications of nano-fibers in the paper by G. Liu, L. Qiao, A. Guo, Macromolecules 29 (1996) 5508.
[54] A. Gomez, K. Tang, Phys. Fluids 6 (1994) 404.
[55] K. Tang, A. Gomez, J. Colloid Interface Sci 175 (1995) 326.
[56] K. Tang, R.D. Smith, Int. J. Mass Spectrom. 162 (1997) 69.
[57] R.J. Pfiefer, C.D. Hendricks, AIAA J. 6 (1968) 496.
[58] J. Fernandez de la Mora, I.G. Locetales, Fluid Mech. Res. 243 (1994) 561.
[59] A.M. Gannan-Calvo, J. Aerosol. Sci. 25 (1994) 309 (suppl. 1).
[60] M.S. Wilm, M. Mann, Int. J. Mass Spectrom. Ion Processes 136 (1994) 167.
[61] N.A. Fuchs, Evaporation and Droplet Growth in Gaseous Media, Pergamon, New York, 1959.
[62] N.B. Zoloti, G.V. Karpov, V.E. Skurat, Sov. Phys. Tech. Phys. 33 (1988) 193.
[63] J.E. Jones, in A. Lakhtakia (Ed.), Essays on the Formal Aspects of Electromagnetic Theory, World Scientific, Singapore, 1993, p. 228.
[64] W.S. Hinds, Aerosol Technology, Wiley Interscience, New York, 1982, Chap. 15.